JTTEE5 19:990–1000
DOI: 10.1007/s11666-010-9502-3
1059-9630/$19.00 © ASM International

Study of the Splat Formation for HVOF Sprayed NiCr on Stainless Steel Substrates and the Effects of Heating and Boiling Pre-Treatments

S. Brossard, P.R. Munroe, and M.M. Hyland

(Submitted November 19, 2009; in revised form February 21, 2010)

The HVOF process is a widely applied thermal spray technique used to form dense coatings with high bond strength. However, little is known about the mechanisms by which the coating forms and adheres to the substrate. The present study investigates the splat formation process by examining the morphology and microstructure of NiCr single splats sprayed on to stainless steel, using a range of electron microscopy techniques. Notable features include evidence of the deformation of the steel substrate by the impacting particle, the presence of porosity towards the centre of the splat, and under the rim due to the curling-up of the splat, and the identification of several oxide phases, including Cr_2O_3, FeO and NiO. From these observations, a description of the splat formation process is proposed. Effects of the substrate surface chemistry were studied by comparing the morphology of the splats on several substrates having undergone various pre-treatments.

Keywords HVOF spray, interface, nickel chromium, oxide, splat, stainless steel

1. Introduction

The high-velocity oxy-fuel (HVOF) spray process allows the manufacturing of coatings of a very wide range of materials (ceramics, metallic alloys, polymers) on a range of substrates, by spraying a fine powder through a mixed oxygen/fuel gas (hydrogen, heptane, kerosene, etc.) flame. The coatings produced, typically, have high bond strength and a dense microstructure in comparison to other thermal spray processes for which particles may be sprayed at higher temperature and lower velocities. Other advantages include higher coating thickness capacity, a smoother surface finish, a lower porosity content, and a lower concentration of oxides in the coating (Ref 1, 2).

Many properties (mechanical, thermal, dielectric, resistance to corrosion, etc.) of the finished coating depend significantly on its microstructure and its interaction with the substrate. Microstructures of thick HVOF coatings have been widely studied (Ref 3-5) and it has been shown that they depend on several factors, such as the feedstock powder and spray conditions (Ref 6, 7). The mechanisms of coating formation are, however, not fully understood. Studying single splats, specifically their formation and their interaction with the substrate, is essential in obtaining a more complete understanding of coating formation to allow optimization of spray conditions.

One notable characteristic of the HVOF process is that, depending on the materials used as feedstock powder (nature and size), the substrate (particularly its hardness) and on the spray conditions (which influence particle temperature and velocity/momentum), splats may form on the substrate either in a fully melted state, in a partially melted state or in an non-melted (i.e. solid) state (Ref 6, 7). These three different states may then be found to be present together within a single coating, giving the coating a bimodal microstructure with a mixture of melted and non-melted zones (Ref 3-5).

Splat formation, in circumstances where the particle impacts on the substrate in a non-melted state, may be compared with the cold spray process. That is, the interaction between substrate and particle upon impact depends significantly on the particle velocity or momentum; if the particle velocity is above a critical value, the particle and/or substrate will undergo plastic deformation as the kinetic energy of the particle is transformed into mechanical deformation and thermal energy. Adhesion of the particle on to the substrate may include the phenomena of mechanical interlocking and adiabatic shear instability (i.e., there is localized deformation at the particle-substrate interface) (Ref 8-10).

Conversely, the situation where the particles impact the substrate in a fully melted state may be more readily compared to the plasma spray process. Splat formation for this process has been more widely studied through

S. Brossard and **P.R. Munroe**, School of Materials, University of New South Wales, Sydney, NSW 2052, Australia; and **M.M. Hyland**, Chemical & Materials Engineering Department, University of Auckland, Auckland 1142, New Zealand. Contact e-mail: sophie.brossard@student.unsw.edu.au.

modeling, studies of splat splashing, and investigations of the possibility of substrate melting (Ref 11-16).

However, studies on the splat formation specifically associated with the HVOF process, in particular where the particles impact the substrate in a semi-melted state, are relatively limited. Trompetter et al., who HVAF sprayed NiCr particles on to a range of substrates with differing hardnesses, observed three distinct types of splats, ranging to fully melted to non-melted, and that their proportion was influenced by the substrate hardness. However, they did not investigate, in detail, either the splat microstructure or the splat-substrate interface (Ref 17). Another study performed by Guilemany et al. examined the substrate-coating interface for a fully deposited WC-Co coating HVOF sprayed on both a polished and a grit-blasted Cu substrate. They found that at the coating-substrate interface a layer of very fine grains. The layer thickness was thinner for the smooth substrate and somewhat thicker for the grit-blasted substrate. This was interpreted as evidence of substrate melting upon impact of the WC-Co particles (Ref 18). Lastly, a model proposed by Sobolev et al. studied the effect of in-flight oxidation of the particle on the splat formation during the HVOF process, leading to the conclusion that this oxidation leads to an increase in splat thickness, with a decrease in both the splat radius and in the pressure developed upon impact. As a result, the splat and substrate made less contact and consequently a decrease in the adhesion and increase in porosity was observed. However, this effect was noted to be in competition with an increase in the wetting of the splat on the substrate due to the oxygen dissolved in the particle (Ref 19).

This study was motivated by the current lack of understanding concerning the splat formation in the HVOF process and the influence of surface chemistry on this process. In this study, NiCr (an alloy often used in thermal sprayed coatings as bond coat or for protection of steel against heat, corrosion (Ref 20), erosion, for example in boilers (Ref 2)) was HVOF sprayed on to stainless steel substrates. These substrates underwent various pre-treatment, such as polishing, heat treating and/or boiling in distilled water. The aim of these pre-treatments was to create different substrate surface conditions in terms of chemistry and roughness. This, then, allowed an investigation of how the substrate conditions may affect splat morphology and the mechanisms of splat formation. The splat microstructure and its interface with the substrate were investigated using a range of microscopy techniques and related to both the spray conditions and substrate chemistry.

2. Experimental Procedure

Four different substrates were used; all prepared from 304 L stainless steel. These are listed in Table 1.

All substrates were first mechanically ground and mirror-polished with diamond paste to a nanoscale roughness. The boiled substrates were placed into boiling distilled water for 30 min, while the thermally treated substrates were heated at 350 °C for 90 min in air. The aim of these treatments is to form surface oxides (or hydroxides for the boiled specimens) and/or to induce some level of surface roughness. All treatments were performed at least several hours before spraying.

Table 1 Substrate nomenclature and condition

Specimen	Substrate	Pre-treatment
SS_P	Stainless steel 304	Polished (to a nanoscale smoothness)
SS_PT	Stainless steel 304	Polished and thermally treated
SS_B	Stainless steel 304	Boiled
SS_BT	Stainless steel 304	Boiled and thermally treated

The sprayed material was a commercial NiCr alloy powder (Ni80-Cr20, Sulzer Metco 43 VF-NS, Switzerland (+45, −5 μm)). HVOF spraying was carried out with a Sulzer Metco (Switzerland) Diamond jet (DJ-2600) gun, fuelled with air at 160 psi and propylene at 110 psi. The feeding rate of the powder was of 26 g/min, the carrier gas being nitrogen at 140 psi. A single swipe pass was made, at the velocity of 0.4 m s^{-1}, and at a spray distance of 266 mm.

The specimens were then characterized using a range of analytical techniques. A Hitachi S3400 scanning electron microscope (SEM) was used to image the overall morphology of the splats and the substrates. A FEI xP200 Focused Ion Beam microscope (FIB) was used to mill cross-sections of the splats using an energetic gallium ion beam, and to image them using secondary electrons induced by the ion beam. Details have been described elsewhere (Ref 21). A FEI xT Nova Nanolab 200 dual beam microscope (that is a FIB and SEM combined into a single instrument) was used to prepare cross-sections of splats (100-200 nm in thickness) suitable for TEM observation. These were prepared using the lift out method as described elsewhere (Ref 21) and examined in a Philips CM200 transmission electron microscope (TEM) to which energy dispersive x-ray spectroscopy (EDS) facilities have been interfaced.

A number of FIB and TEM cross-sections were made and studied, at least one for each particular feature and/or type of splat, but only a small number of representative images will be presented here. The preparation of cross-section involves the deposition of a layer of platinum on top of the area of interest prior to milling for protection purposes. This layer is then present in the images shown here.

3. Results and Discussion

3.1 Description of the Different Types of Splats Observed by SEM

SEM images of 50-60 splats were observed for each specimen. From these observations it was noted that the

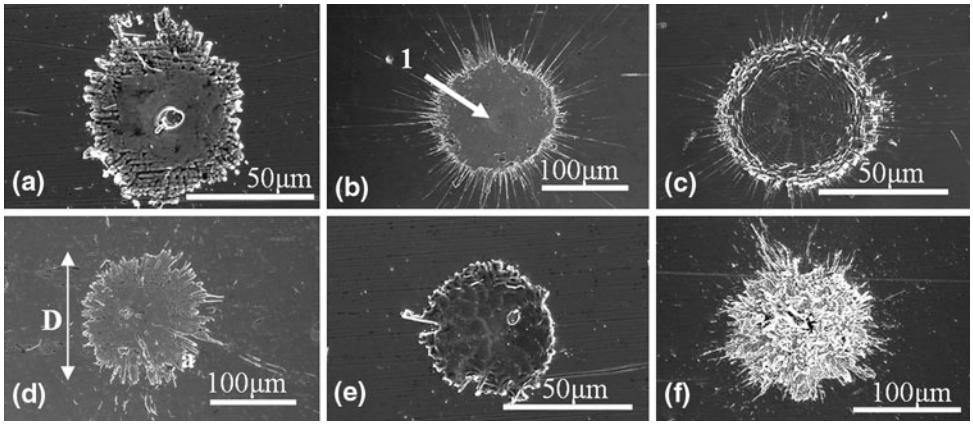

Fig. 1 SEM images of the different types of splats: large fully melted splat (a) with an irregular dendritic/granular rim, (b) with a smooth rim and thin splashed fingers, (c) with a rim displaying an undulating surface, (d) with an irregular rim with radial cracks, (e) small circular splat, (f) partially melted splat

majority of the splats observed, for the all four substrates, appeared to be formed from fully melted NiCr and presented a mainly disc-shaped morphology. Figure 1 presents typical SEM images of the different splats found for the various substrates. Amongst these splats, two types can be seen: large fully melted splats (diameter between 30 and 200 μm, see Fig. 1a-d), with a shallow depression in their centre (marked 1 on Fig. 1b), and small fully melted splats (diameter usually between 10 and 30 μm, see Fig. 1e), with no depression observed. Evaluating the diameter D was performed by taking the smallest and largest diameter value measured from the splat, which is not perfectly circular, and calculating the average value; features such as splashed fingers were ignored (see for example Fig. 1d). The large fully melted splats shown were found to present differences principally in the morphology of their rim, which may be either significantly irregular, with a granular or dendritic aspect (Fig. 1a), or quite smooth with thin splashed fingers (Fig. 1b), or smooth with a surface that has become irregular and undulating (Fig. 1c) or finally very irregular with some radial cracks (Fig. 1d).

For the all four substrate conditions, a small number of splats (~8%) appeared to have formed from a partially melted particle. Figure 1(f) displays a SEM image of such a splat. These are usually disc-shaped; such splats apparently consist of a mixture of non-melted fragments within a melted matrix. Their diameter ranged from ~70 to ~210 μm.

3.2 Structure and Formation of the Large Fully Melted Splats

3.2.1 Description of their Microstructure as Observed by FIB and TEM. For these large fully melted splats, a number of characteristics features were observed which were noted for all four substrates.

Firstly, the substrate at the centre of these splats always exhibited a depression, or shallow crater. For example on the FIB cross-section presented Fig. 2, towards the centre

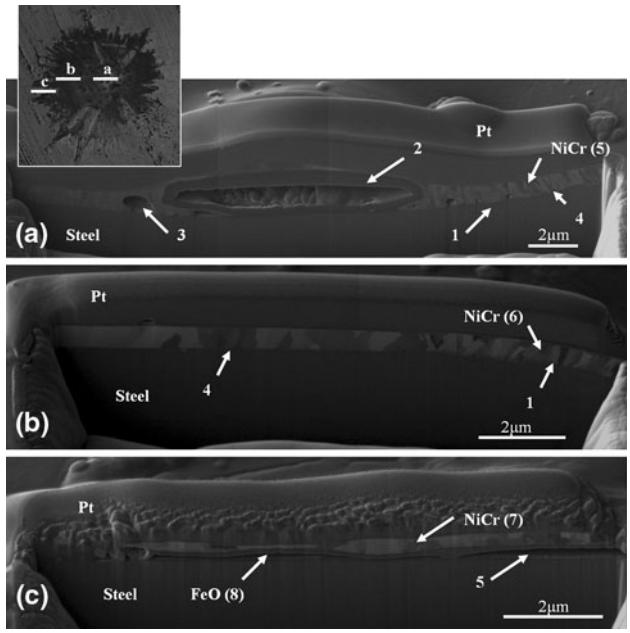

Fig. 2 FIB cross-sections on a fully melted splat with an irregular rim (the inset image shows an image of the splat in plan view before sectioning) found on SS_P: (a) across the centre, (b) across the rim of the crater and (c) across the rim of the splat

of the splat it can be noted that the splat-substrate interface is curved (marked 1). Also, porosity is almost always found towards the centre of the splats, near the splat-substrate interface. For the cross-section in Fig. 2, at the centre of the splat, a large single pore (marked 2), together with a number of some smaller pores (marked 3), can be observed. Large pores were not always present. Instead, some smaller pores may be observed, such as for the splat whose TEM cross-section is displayed in Fig. 3 (marked 1).

Another important feature is the splat-substrate interface. In the large fully melted splats, the contact between

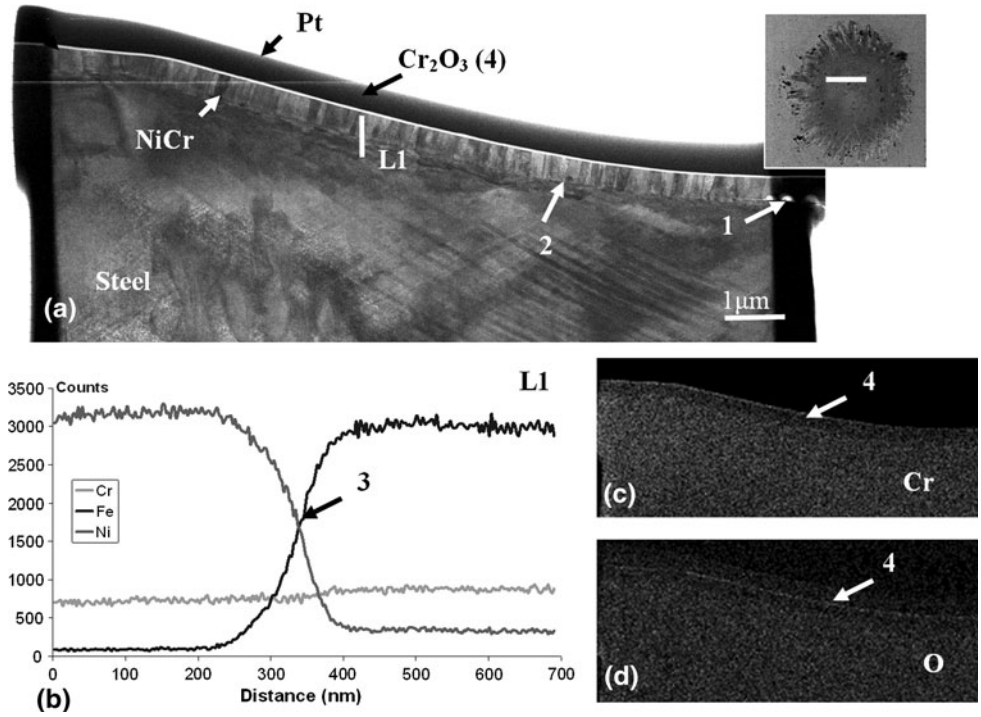

Fig. 3 TEM cross-section across the centre of a fully melted splat found on SS_P (see inset image): (a) bright field image, (b) elemental linescan across the splat-substrate interface at the region L1, elemental maps for (c) Cr and (d) O

splat and substrate was usually very good, such as for example Fig. 2 (marked 4), at least away from the rim of the splat. TEM study of the splat-substrate interface, for example Fig. 3, shows that the interface appears quite distinct in the bright-field TEM images (marked 2). However, the elemental linescan performed across the same interface showed the presence of an interdiffusion zone between Ni and Fe over distances of up to 200 nm, depending on the exact location of the linescan. In most cases, the interdiffusion is significant where the interface becomes slanted towards the periphery of the crater (marked 3 on Fig. 3, 150 nm), while there is no, or limited, interdiffusion, observed at both the centre of the splat or closer to the splat rim.

The splats' rims, as noted in the SEM images, may differ from splat to splat. On Fig. 2(c), one can observe the structure under an irregular rim, where delamination has clearly occurred (marked 5). On the other hand, Fig. 4 displays a FIB cross-section of the rim of a splat showing an undulating outer surface towards the splat periphery (marked 1). Here, the contact between substrate and splat is good (marked 2).

Observation of the grain structure is consistent with the previous comments. For example in Fig. 2, inside the crater the grain structure is fine and columnar (marked 6), which is consistent with the good contact between splat and substrate, since this is an indication of rapid solidification and effective removal of the heat through the substrate. Towards the periphery, however, the grain structure becomes coarser and more equiaxed (marked 7): the solidification rate in this region must have been lower

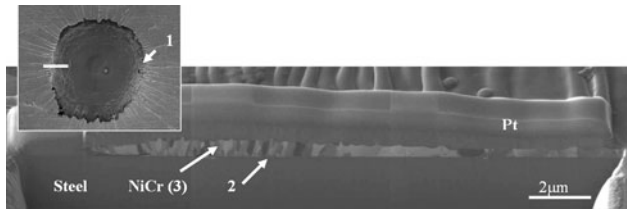

Fig. 4 FIB cross-section across the rim of a splat found on SS_PT and presenting a undulating outer surface close to the splat periphery (see inset image)

and, correspondingly, the contact between splat and substrate is poorer (marked 5), preventing efficient heat removal through the substrate. On Fig. 4, however, the contact is better at the periphery, thus the grain structure is much finer (marked 3).

Several oxide phases were identified in characteristic locations around the splat. First, nickel and iron oxides were found to often form in the pores found at the centre of the splats. In large pores, a thick and dense layer was often observed to cover the walls of the pores, such as that seen on Fig. 2 (marked 2), but also visible on Fig. 5 (marked 1). Such a layer was identified using TEM as being FeO: the EDS elemental maps (see Fig. 5d and e) show that Fe is present in the layer (O is present as well, but EDS is less sensitive to the presence of oxygen), and the electron diffraction pattern obtained from this region is consistent with FeO (see diffraction pattern, Fig. 6a). NiO was found to be more prone to

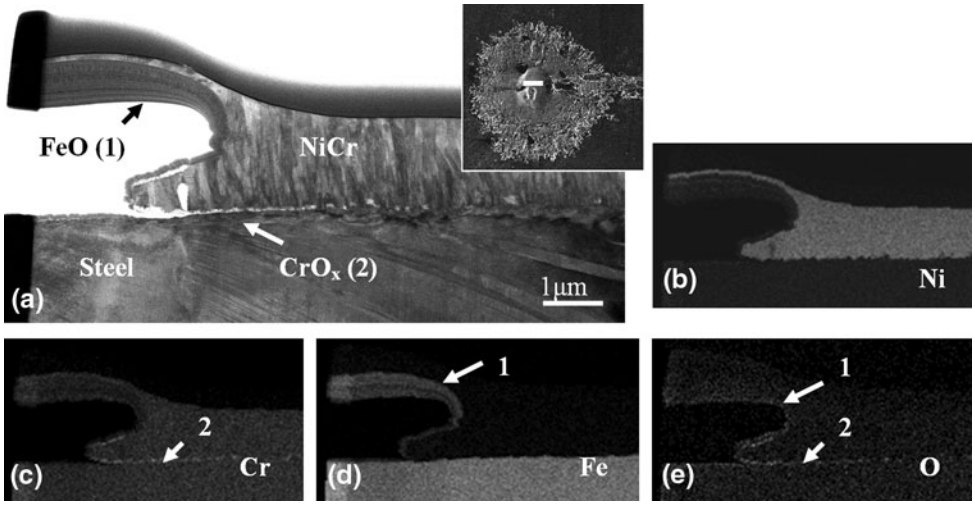

Fig. 5 TEM cross-section across the centre of a fully melted splat found on SS_P (see inset image) and presenting a large central pore: (a) bright-field image and elemental maps of (b) Ni, (c) Cr, (d) Fe and (e) O

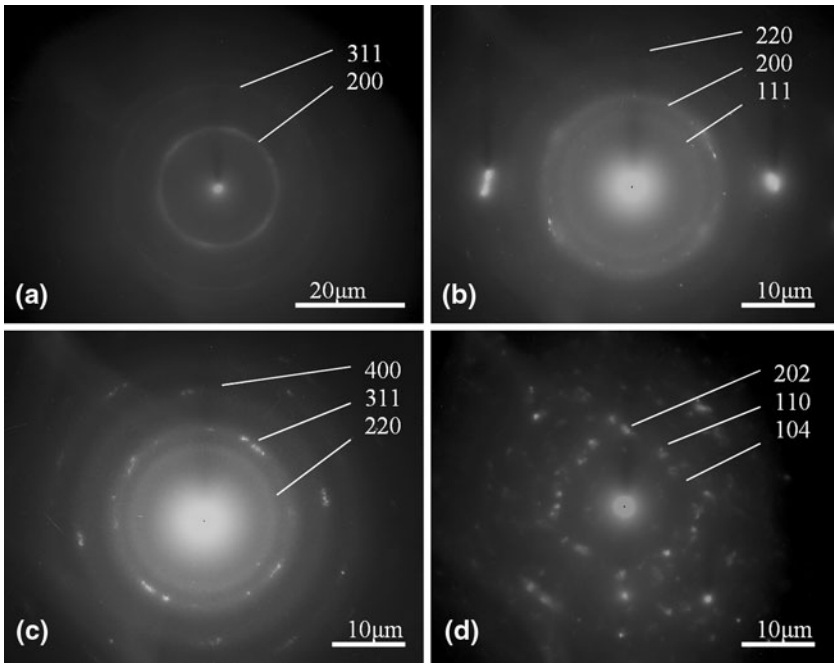

Fig. 6 Diffraction patterns of the different oxides found: (a) FeO, (b) NiO, (c) $NiCr_2O_4$, (d) Cr_2O_3

form in the smaller pores, for example on the TEM cross-section shown in Fig. 7 (marked 1). $NiCr_2O_4$ spinel was also found in similar locations in other, similar splats. Both types of oxides were identified using EDS, together with electron diffraction methods (see their diffraction patterns shown in Fig. 6b and c). More detail on the identification of oxide phases in NiCr splats on steel substrates using TEM can be found elsewhere (Ref 16). Furthermore, at the periphery of splats where delamination is observed, a layer of oxide was often seen on the lower surface of the splat, such as on Fig. 2 (marked 8). Identification by TEM-EDS and electron diffraction showed that this phase was FeO.

Finally, it was often found that a thin layer of Cr oxide is present on the outer surface of the splats (marked 4 on Fig. 3 and 2 on Fig. 7). When this layer was thick enough for an electron diffraction pattern to be readily obtained, it was identified as Cr_2O_3 (see diffraction pattern Fig. 6d), which is, indeed, the Cr oxide phase most likely to be formed on these splats (Ref 22, 23). In some cases, the layer of Cr_2O_3 was notably thicker and appears to have cracked upon cooling and solidification due to thermal

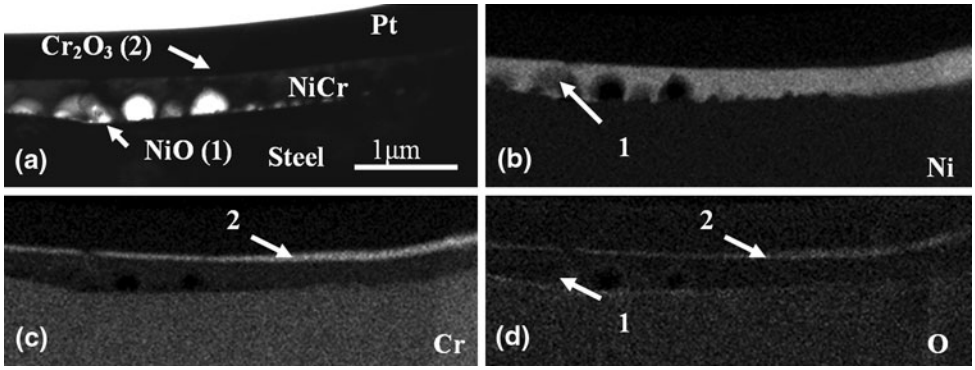

Fig. 7 TEM cross-section across the centre of a fully melted splat found on SS_BT presenting small pores at the splat-substrate interface with NiO: (a) bright-field image and EDS elemental maps of (b) Ni, (c) Cr, (d) O

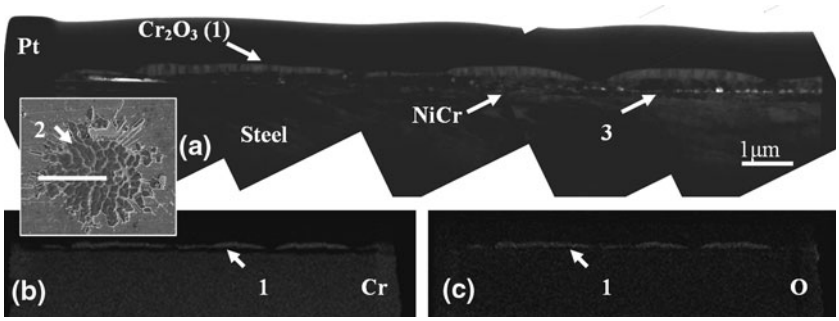

Fig. 8 TEM cross-section of a small fully melted splat (see inset image) from the SS_BT specimen: (a) bright field image and elemental maps for (b) Cr and (c) O

expansion mismatch (chromium oxide coefficient of thermal expansion is ~7 μm/m · °C (Ref 24), in comparison to ~16 μm/m · °C for NiCr (Ref 25)), as it can be observed on the TEM cross-section displayed in Fig. 8 (marked 1), made on a small fully melted splat (a similar structure was found on some large fully melted splats). This phenomenon creates the patterns of cracks that can be observed on the outer surface of some splats (marked 2 on the inset SEM image in Fig. 8). Chromium oxide was also observed by EDS mapping at the splat-substrate interface, for instance in Fig. 5 (marked 2), but in such cases it could not be unambiguously identified by electron diffraction. This oxide may arise from either the oxidation of the steel substrate (Ref 26, 27), or the oxidation of the splat.

3.2.2 Description of the Splat Formation Process. FIB and TEM cross-sections of these splats did not reveal the presence of any non-melted remnants from the original sprayed particle. However, this may not mean that the sprayed particle was completely molten when it impacted on the substrate. Indeed, analysis of similar fully melted splats prepared by plasma spray processes (Ref 15) showed that in this case the substrate shows no evidence of deformation. However, in this study the observation of a shallow crater indicates that the substrate must have been deformed by the impinging particle. Substrate deformation, observed usually for the cold spray process where the particles impact the substrate in a solid state, has also been observed to varying degrees for HVOF in a number of previous studies and, therefore, is not unexpected (Ref 17, 28, 29). The deformation of the substrate is attributed to the ''peening effect'', is said to lead to an increased adhesion of the coating by inducing a high level of compressive residual stress in the coating (Ref 28-30).

Zhang et al. noted, for HVOF sprayed particles in a partially melted state, that they were comprised of a non-melted core surrounded by a layer of melted material (Ref 31). Based on the hypothesis that the NiCr particles impacted the steel substrate in such a state, the non-melted core could then have been responsible for the substrate deformation observed. This brings the question of the behavior of the non-melted components following impact.

Previous studies have shown that further melting may have occurred upon impact from the transformation of the kinetic energy of the particle in heat and plastic deformation (Ref 17). However, this may account for only a limited volume of material. Diameters of the largest splats are around 200 μm, and examination of the FIB and TEM cross-sections showed that the thickness of the splats may be up to 2 μm. An estimate of splat volume would, therefore, correspond to the volume of a sphere of diameter of around 24 μm. This is far less than the maximum diameter of the feedstock powder (45 μm).

A possible explanation may be that the non-melted core may have rebounded from the substrate upon impact.

Study of the cold spray process showed, indeed, that for a solid Ni particle to adhere on steel, it must impact the substrate with a velocity superior to a critical velocity of 640 $m \cdot s^{-1}$ (Ref 32). Considering the range of impact velocity that is typical for HVOF (400-800 $m \cdot s^{-1}$ (Ref 1)), this velocity may not be achieved on primary impact of the particle and is certainly unlikely to be achieved on secondary impact after a rebound. Thus, the solid core, if it has rebounded away the substrate, does not subsequently adhere to the substrate.

One may note though that the splats are fully contiguous: there is not evident sign of the rebound of a solid core. Another possibility would be then to consider the fact that smaller particles impact on the substrate in a more molten state compared to larger ones (Ref 6). The largest particles could then have simply not adhered to the substrate because they impacted in a mostly solid state. However this would lead to the presence of many impact marks on the substrate, while only very few of these were observed. Consequently, the hypothesis of the rebound of a solid core is more plausible, and the absence of evidence of rebound in the shape of the splat may be explained by the solidification rate of the splats which may have been slow enough to allow the molten NiCr splat to smoothen.

It was observed that some splats displayed a large central pore, for example as seen in Fig. 2 and 5. Porosity at the splat-substrate interface is often found in the case of plasma sprayed specimens: it was then hypothesized that such pores may partly form due to gas release from the substrate particle impact and flattening due to desorption of asdorbates/condensates present on the surface of the substrate (Ref 11, 15, 33). A similar phenomenon was also studied by Sobolev et al. in the case of HVOF sprayed coatings (Ref 34). Gases may also be entrapped under the impacting droplet (Ref 35) or be released after having been dissolved within the liquid droplet (Ref 33). However, the amount of these gases is limited and some pores observed here are significantly large (a few μm in diameter). Modeling of splat formation in plasma spraying has also shown that due to the mechanics of flow of the melted particle (change of curvature in the droplet) a large open central pore was found to form (Ref 36, 37). This may be applicable to the HVOF study here, with the difference being that the pore remains closed, possibly due to the lower temperature of the splat and the better contact between splat and substrate leading to a faster solidification, which would not leave sufficient time for the pore to become unstable and burst open.

Some other splats display some fine porosity in their centre near the splat-substrate interface, for example in Fig. 7. In such cases, gas release is most probably the cause of their formation. The presence of oxides, such as NiO, within these pores supports this hypothesis, as it shows that hot oxidizing gases must have been present within these pores. Moreover, if gas release indeed occurs, this should take place all along the splat-substrate interface. However, porosity is only observed at either the centre of the splat or towards its periphery. The gas released must then be pushed in direction of the periphery of the splat by the flowing melted NiCr during splat flattening. This would cause the presence of hot oxidizing gases at the splat-substrate interface under the rim of the splat. At this location delamination of the splat is often observed and a layer of FeO on the bottom surface of the splat: possibly when the flattened splat solidifies and cools down, curling up of the rim occurs to accommodate the thermal stress rising from the decrease in temperature, leading to the lift-up of the rim of the splat (Ref 34, 38). On the bottom surface of the splat being lifted up, some Fe must have deposited from the steel substrate, which then is oxidized by the hot gases from the gas release described previously.

Finally, a common feature of the splats observed was the interdiffusion of NiCr and steel across the splat-substrate interface, even though the images showed that the interface appeared straight and distinct in structure. Diffusion across the interface may not be indicative of substrate melting. Indeed, if localized melting of the substrate had taken place, variations in the splat-substrate interface would likely have been observed (Ref 16), which was not the case here. Thus, the diffusion observed must arise from the very good contact between splat and substrate and the diffusion of the heat from the melted NiCr into the substrate. This is also consistent with the observation that the degree of interdiffusion observed (usually around 200 nm) is quite limited. It should also be noted that diffusion is maximum on the slanted walls of the crater, while it does not occur at the centre of the splat or at the periphery. At these locations, the contact between splat and substrate is poor possibly because of the porosity formation for the centre of the splat, and the decrease of the pressure applied by the impacting and flowing particle on the substrate towards the periphery. Consequently, it is expected that no, or limited, diffusion occurred there.

Figure 9 displays a schematic representation summarizing the splat formation process: upon impact the substrate gets deformed by the non-melted core (1), while the melted NiCr starts spreading to form a splat (2), then the non-melted core rebounds (3). In the centre a large pore may form (or alternatively a number of smaller pores) (4), while the melted NiCr spreads, pushing outwards gas that may be released from the substrate (5), and interdiffusion across the splat substrate interface takes place (6). In the end, curl-up of the splat occurs at its periphery (7) and

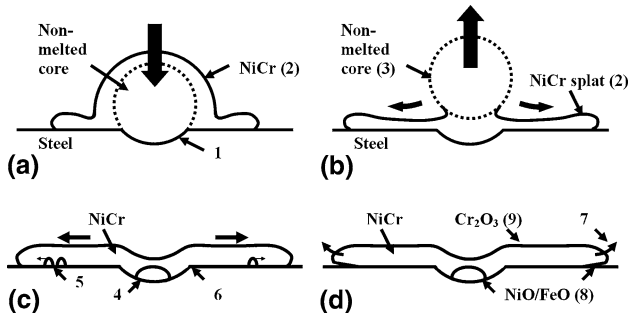

Fig. 9 Schematic representation of (a) a Ni-Cr particle impacting on the steel substrate and (b) the non-melted core rebounding from the substrate, then (c) the splat flattening and (d) solidifying and cooling down

oxides (FeO, NiO…) may form in the central pore and/or under the rim of the splat (8). Cr oxide was also found to form as a thin layer on the outer surface of the splat (9).

3.3 Structure and Formation of the Small Fully Melted Splats

Such splats have typically a diameter ~30 μm and a thickness of ~0.5 μm. The volume of these splats corresponds to an initial spherical particle of diameter of ~9 μm. They would then most probably originate from the smallest particles of the feedstock powder.

For these splats, their structure is quite similar to that of the larger fully melted splats, in terms of grain structure, porosity and oxide phases. However, some noticeable differences were found: firstly, as it can be seen in Fig. 8a (marked 3), no crater or evidence of substrate deformation was observed. Consequently, unlike the large splats described in the previous section, it is probable that the NiCr particle was fully melted when impacting the substrate, which is consistent with the observation that smaller particles undergo further melting than the larger ones. Also, no interdiffusion was detected across the splat-substrate interface (marked 3 on Fig. 8a). This could be linked to the thinness of the splats leading to rapid solidification, hindering the occurrence of interdiffusion, the small size of the particles meaning a lower momentum upon impact, and also to the absence of substrate deformation, which shows the pressure applied by the impacting particle on the substrate was limited.

3.4 Structure and Formation of the Partially Melted Splats

FIB cross-sections of a partially melted splat, similar to that shown in Fig. 1(f), confirmed the assumption that they comprise a mixture of non-melted fragments in a matrix of NiCr that had melted. Figure 10 presents two cross-sections on such a splat. A mix of fine grains (marked 1, $d < 1$ μm, from the phase that was fully melted) and very large grains (marked 2, $d \sim$ 2-10 μm, probably originating from the non-melted particle) can be observed. The melted phase allows the splat here to have a good contact with the substrate (marked 3). However, some pores were observed close to the splat periphery, possibly due to a lack of melted material to fill them (marked 4). On some other splats the voids were found to be significantly large (<10 μm) and towards the centre of the splat. When examining the splat-substrate interface, especially towards the centre of the splat, one can note that it is slightly curved (marked 5). This is due to the deformation of the substrate by the impact from the particle, forming a shallow crater.

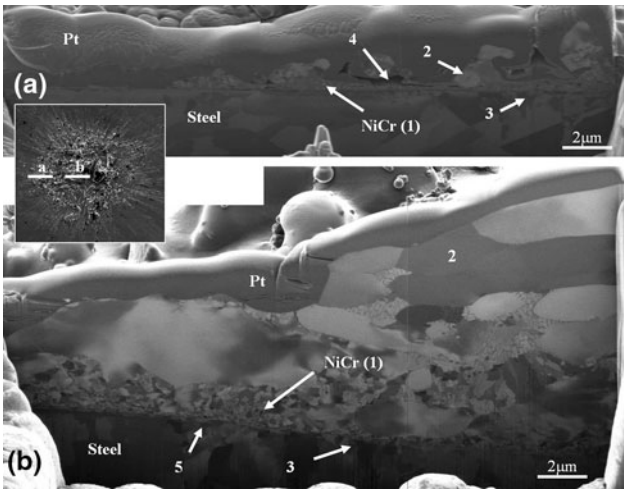

Fig. 10 FIB cross-sections of a partially melted splat (see inset image), found on SS_B, (a) across the periphery and (b) towards the centre of the splat

Chemical analysis using EDS in the TEM did not show the presence any particular oxide phase. One may expect some of the oxides that have been observed on the fully melted splats, such as NiO, FeO or $NiCr_2O_4$; presumably these oxides, if present, were in such small amounts that they were not detected using TEM.

Such splats, compared to the large fully melted splats, display a shallow central crater as well, showing that deformation has also occurred. However, the partially melted splats are much thicker and display large non-melted fragments embedded in a fine grained matrix that appears to have been fully melted upon splat formation. Consequently, it seems that such splats were formed from the impact of a partially melted particle, the non-melted core causing the deformation of the substrate, in the same way as the fully melted splats, except such a core may break up upon impact, the fragments being then embedded within the melted NiCr. This large thickness, however, inhibits the preparation of TEM specimens that allows ready observation of any oxide phase or interdiffusion across the splat-substrate interface.

3.5 Effects of the Pre-Treatments on the Splat Morphology and Formation

Stainless steel exhibits on its surface very thin layers of oxide comprising an outer layer of mainly of Fe_2O_3, and an inner layer of mainly of a mixture of Cr and Fe oxides (Cr_2O_3, Fe_2O_3, spinel type $Fe(Fe,Cr)_2O_4$ or $Ni_xFe_{3-x}O_4$) (Ref 26, 27)). X-ray photoelectron spectroscopy (XPS) studies also showed that some hydroxide may be present on the surface (Ref 39). Previous studies for plasma sprayed NiCr showed that heat treatment of a steel substrate may result in increasing the oxide content, converting, for example, the hydroxide into oxide, and/or thickness of this oxide layer (Ref 15). Cedelle et al. found that substrate heat treatment also resulted in a positive skewness, which accounted for the better wetting of the plasma sprayed Ni splats and a shorter spreading time (Ref 40). On the other hand, boiling stainless steel is expected to increase the hydroxide content (FeOOH) of the oxide layer. In any case, the oxide/hydroxide layers before spraying are very thin (less than a few nanometers) (Ref 15). The heat and boiling treatments were also found to slightly increase the nanoscale roughness of the steel specimens (Ref 15).

For each specimen, SEM images of 50-60 splats were taken and for each type of splat the average diameter and their relative proportions were evaluated. Examination of the splat population for each of the different substrates conditions showed that the relative proportion of the partially melted splats was consistent (~8%). For the small fully melted splats, their proportion is more variable, usually between 10 and 20% of the splats observed. However, both categories did not present significant variations between the various substrates.

Conversely, the fully melted splats were found to differ between the different specimens, but only by the morphology of their rims. The central part of the splat was always broadly similar. This suggests that formation of this central portion is mainly governed by the mechanics of the melted (or partially melted) NiCr impacting with a high kinetic energy on the substrate, thus, with building up of a high pressure at the interface with the substrate, undermining the possible effects of the surface chemistry. However, towards the periphery of the splat, where the pressure applied by the melted NiCr on the substrate becomes minimal, surface chemistry may influence the wetting of NiCr, thus the manner in which the splat spreads and in the differences in rim morphology.

Table 2 summarizes the different rim morphologies that were observed along with the approximate mean diameter of the splats, along with the standard deviation of the diameters. Despite the uncertainties, some trends can be observed. When observing plasma sprayed splats on similarly treated steel substrates, it was found that the heat-treatment improved the wetting of NiCr on steel, giving flatter splats (Ref 15, 40). It seems here that the heat-treatment may have had a similar action: by the improving the wetting of NiCr on steel, the splats were flatter, thus with a larger diameter, and with a better contact with the substrate towards the periphery, thus being less prone to delamination and the formation of cracks during cooling. The undulations observed on the surface at the rim also indicate wetting and contact: it seems that the flow of molten NiCr becomes retarded and stopped by the friction from the intimate contact with the substrate. This is possibly due to the fact that the increase in the oxide content and nanoscale roughness/skewness of the surface produced by the heat-treatment (Ref 15, 40) improves the wetting of NiCr on steel and also decreases the amount of adsorbates/condensates on the substrate, thus less gas is released from the substrate upon splat formation and the contact between the splat and the substrate is improved (more details on the effects of heat-treating on the surface chemistry may be found in a previous work by the same authors; Ref 15). The splashed fingers may also be caused by the increased nanoscale surface roughness.

Table 2 Various splat morphologies and corresponding average diameters for the splats found on the different specimens

Specimen	Description of the large fully melted splats	Average diameter
SS_P	Irregular dendritic/granular rim (Fig. 1a)	[65 ± 21] μm
SS_PT	Rim ranging from smooth with thin splashed fingers to circular with an undulating surface (Fig. 1b and c)	[86 ± 38] μm
SS_B	Irregular rim with radial cracks (Fig. 1d)	[83 ± 41] μm
SS_BT	Rim ranging from irregular with radial cracks to circular with an undulating surface (Fig. 1c and d)	[91 ± 32] μm

The boiling treatment also appears to significantly increase the splat diameter, but splats tend to display an irregular rim prone to delamination and radial cracks. Such cracks may be linked to this increase in diameter: the splats would be indeed much thinner, including regions towards the splat periphery, and thus more prone to cracking.

However, the manner in which boiling the substrate creates the morphologies observed is not clear. Possibly, the increase in the FeOOH content of the steel surface causes on one hand a slight increase in nanoscale roughness/skewness, which may improve the wetting of NiCr, but on the other hand, due to the dehydration of the hydroxide upon splat formation, more gas may be released from the substrate upon splat formation, hindering the contact between splat and substrate and causing the irregular morphology of the rim.

In summary, pre-treatments influence splat formation and morphology through modifying the surface chemistry and roughness, but this affects splat morphology mainly towards their periphery. No significant effect on the oxide content and the porosity formed towards the centre of the splat was found. On the other hand, it is possible that porosity formed due to the delamination under the rim may be affected by the pre-treatments. Porosity, along with the oxide content, are known to be significant features which influence the properties of the fully deposited coating, such as thermal and dielectric conductivity or resistance to corrosion (Ref 7, 20, 31). However, as the effects of the pre-treatments on porosity and oxide is limited, such pre-treatments of the substrate may not be very influential factors on the final properties of the HVOF sprayed coatings, especially compared to other spray conditions factors such as the temperature and velocity of the particles.

When comparing with plasma sprayed NiCr splats on similar substrates (Ref 15), HVOF splats can be noted to present interesting points of difference. For example, in HVOF the amount of oxide is reduced. Regarding the porosity, the amount of small pores (<1 μm) is significantly reduced for the HVOF splats, but the central pores are larger than the ones usually observed for the plasma splats. This may be explained by a stronger influence, in their formation process, of the mechanics of the flow of the liquid splat, compared to the gas release phenomenon. Further, despite the absence of evidence of substrate melting, as found for plasma sprayed splats, the contact between splat and substrate is usually better. In HVOF the splat shapes are also more uniform and regular, as plasma sprayed splats in most cases tend to be more fragmented and splashy. Finally, the depression from the

impact of the particle and the formation of very large central pores are characteristic of HVOF splats, as there is no deformation of the substrate in the case of plasma spray and the pores found in the centre of the splats are much smaller and caused mainly by the presence of gas. It is consequently logical that HVOF coatings are often found to be denser and with lesser oxide content compared to plasma coatings (Ref 2).

4. Conclusion

In conclusion, the study of HVOF sprayed NiCr single splats on stainless steel, and the comparison of their morphology depending on the pre-treatment of the steel substrate, lead to the following observations:

- The sprayed particle impacts the substrate in a partially molten state, and its solid core caused the deformation of the substrate, thus the formation of a shallow crater.
- In the case of the fully melted splats, the solid part of the sprayed particle rebounds from the substrate. In the case of the partially melted splats, some non-melted fragments remain embedded in a matrix of melted NiCr. In both cases, only a fraction of the initial particle adheres to the substrate.
- Splats usually display some porosity at the splat-substrate interface in their centre, and also at the periphery where delamination may have occurred. Elsewhere, the contact between splat and substrate is good, and the interdiffusion between Ni and Fe across the interface shows that metallurgical bonding may have taken place.
- Some Cr_2O_3 may form as a thin layer on the outer surface of the splat, while NiO and FeO may be found where porosity has formed.
- Changes in surface conditions induced by the heat and boiling pre-treatments may influence splat formation through the way melted NiCr wets on the substrate and the amount of adsorbates/condensate that may get desorbed from the substrate. However, their effect is quite limited.

To apply high-resolution microscopy techniques to the study of single splats is a novel way of studying thermal spray coatings and has shown to bring a new insight in the splat microstructure and how splats interact with the substrate.

References

1. M. Dorfman, Thermal Spray Basics, *Adv. Mater. Process*., 2002, p 47-50
2. R.F. Bunshah, *Handbook of Hard Coatings. Deposition Technologies, Properties and Applications*, Norwich, NY, 2001
3. P. Bansal, P.H. Shipway, and S.B. Leen, Effect of Particle Impact on Residual Stress Development in HVOF Sprayed Coatings, *J. Therm. Spray Technol.*, 2006, **15**(4), p 570-575
4. C.J. Kong, P.D. Brown, S.J. Harris, and D.G. McCartney, The Microstructure of a Thermally Sprayed and Heat Treated Al-20 wt.%Sn-3 wt.Si% Alloy, *Mater. Sci. Eng.*, 2005, **A403**, p 205-214
5. T. Marrocco, L.C. Driver, S.J. Harris, and D.G. McCartney, Microstructure and Properties of Thermally Sprayed Al-Sn-Based Alloys for Plain Bearing Applications, *J. Therm. Spray Technol.*, 2006, **15**(4), p 634-639
6. J.A. Browning, Hypervelocity Impact Fusion—A Technical Note, *J. Therm. Spray Technol.*, 1992, **1**(4), p 289-292
7. E. Turunen, T. Varis, S.-P. Hannula, A. Vaidya, A. Kulkarni, J. Gutleber, S. Sampath, and H. Herman, On the Role of the Particle State and Deposition Procedure on Mechanical, Tribological and Dielectric Response of High Velocity Oxy-fuel Sprayed Alumina Coatings, *Mater. Sci. Eng.*, 2006, **A415**, p 1-11
8. S.V. Klinkov, V.F. Kosarev, and M. Rein, Cold Spray Deposition: Significance of Particle Impact Phenomena, *Aerosp. Sci. Technol.*, 2005, **9**, p 582-591
9. R.C. Dykhuizen, M.F. Smith, D.L. Gilmore, R.A. Neiser, X. Jiang, and S. Sampath, Impact of High Velocity Cold Spray Particles, *J. Therm. Spray Technol.*, 1999, **8**(4), p 559-564
10. L. Ajdelsztajn, A. Zúñiga, B. Jodoin, and E.J. Lavernia, Cold Gas Spraying of a High Temperature Al Alloy, *Surf. Coat. Technol.*, 2006, **201**, p 2109-2116
11. P. Fauchais, M. Fukumoto, A. Vardelle, and M. Vardelle, Knowledge Concerning Splat Formation: An Invited Review, *J. Therm. Spray Technol.*, 2004, **13**(3), p 337-360
12. H. Zhang, X.Y. Wang, L.L. Zheng, and X.Y. Jiang, Studies of Splat Morphology and Rapid Solidification During Thermal Spraying, *Int. J. Heat Mass Transf.*, 2001, **44**, p 4579-4592
13. L. Li, X.Y. Wang, G. Wei, A. Vaidya, H. Zhang, and S. Sampath, Substrate Melting During Thermal Splat Quenching, *Thin Solid Films*, 2004, **468**, p 113-119
14. S. Kitahara and A. Hasui, A Study of the Bonding Mechanism of Sprayed Coatings, *J. Vac. Sci. Technol.*, 1974, **11**(4), p 747-753
15. S. Brossard, P.R. Munroe, A.T.T. Tran, and M.M. Hyland, Study of the Effects of Surface Chemistry on Splat Formation for Plasma Sprayed NiCr onto Stainless Steel Substrates, *Surf. Coat. Technol.*, 2009, **204**(9-10), p 1599-1607
16. S. Brossard, P.R. Munroe, A.T.T. Tran, and M.M. Hyland, Study of the Microstructure of NiCr Splats Plasma Sprayed on Stainless Steel by TEM, *Surf. Coat. Technol.*, 2009, **204**(9-10), p 1608-1615
17. W.J. Trompetter, M. Hyland, D. McGrouther, P. Munroe, and A. Markwitz, Effect of Substrate Hardness on Splat Morphology in High-Velocity Thermal Spray Coatings, *J. Therm. Spray Technol.*, 2006, **15**(4), p 663-669
18. J.M. Guilemany, J. Nutting, J.R. Miguel, and Z. Dong, Microstructure Characterization of WC-Ni Coatings Obtained by HVOF Thermal Spraying, *Scr. Metall. Mater.*, 1995, **33**(1), p 55-61
19. V.V. Sobolev and J.M. Guilemany, Effect of Oxidation on Droplet Flattening and Splat-Substrate Interaction in Thermal Spraying, *J. Therm. Spray Technol.*, 1999, **8**(4), p 523-530
20. M.E. Aalamialeagha, S.J. Harris, and M. Emamighomi, Influence of the HVOF Spraying Process on the Microstructure and Corrosion Behavious of Ni-20%Cr Coatings, *J. Mater. Sci.*, 2003, **38**, p 4587-4596
21. P.R. Munroe, The Application of Focused Ion Beam Microscopy in the Material Sciences, *Mater. Charact.*, 2009, **60**, p 2-13
22. J. Stringer, B.A. Wilcox, and R.I. Jaffee, The High-Temperature Oxidation of Nickel - 20wt% Chromium Alloys Containing Dispersed Oxide Phases, *Oxid. Met.*, 1972, **5**(1), p 11-47
23. N.S. McIntyre, T.C. Chan, and C. Chen, Characterization of Oxide Structures Formed on Nickel-Chromium Alloy During Low Pressure Oxidation at 500-600°C, *Oxid. Met.*, 1990, **33**(5/6), p 457-479
24. O. Madelung, U. Rössler, and M. Schulz, *Non-Tetrahedrally Bonded Binary Compounds II*, Springer-Verlag, 2006
25. MatWeb, Material Property Data, 2008 11/11/2008; Available from http://www.matweb.com/
26. S.B. Newcomb, "A Microsctructural Study of the Oxidation of Ni-Cr Steels in Air and in CO-CO_2," Ph.D. Thesis, University of Cambridge, 1982

27. G.C. Allen, J.M. Dyke, S.J. Harris, and A. Morries, A Surface Study of the Oxidation of Type 304L Stainless Steel at 600 K in Air, *Oxid. Met.*, 1987, **29**(5/6), p 1988
28. C.-J. Li and Y.-Y. Wang, Effect of Particle State on the Adhesive Strength of HVOF Sprayed Metallic Coating, *J. Therm. Spray Technol.*, 2001, **11**(4), p 523-529
29. T.C. Totemeier, R.N. Wright, and W.D. Swank, Microstructure and Stresses in HVOF Sprayed Iron Aluminide Coatings, *J. Therm. Spray Technol.*, 2002, **11**(3), p 400-408
30. S. Kuroda, Y. Tashiro, H. Yumoto, S. Taira, H. Fukanuma, and S. Tobe, Peening Action and Residual Stresses in High-Velocity Oxygen Fuel Thermal Spraying of 316L Stainless Steel, *J. Therm. Spray Technol.*, 2001, **10**(2), p 367-374
31. D. Zhang, S.J. Harris, and D.G. McCartney, Microstructure Formation and Corrosion Behaviour in HVOF-Sprayed Inconel 625 Coatings, *Mater. Sci. Eng.*, 2003, **A344**, p 45-56
32. A.P. Alkhimov, V.F. Kosarev, and A.N. Papyrch, A Method of Cold Gas Dynamic Deposition, *Dokl. Akad. Nauk. USSR*, 1990, **318**, p 1062-1065
33. M. Qu and A. Gouldstone, On the Role of Bubbles in Metallic Splat Nanopores and Adhesion, *J. Therm. Spray Technol.*, 2008, **17**(4), p 486-494
34. V.V. Sobolev and J.M. Guilemany, Investigation of Coating Porosity Formation During High Velocity Oxy-Fuel (HVOF) Spraying, *Mater. Lett.*, 1994, **18**, p 304-308
35. V. Medhi-Nejad, J. Mostaghimi, and S. Chandra, Air Bubble Entrapment Under an Impacting Droplet, *Phys. Fluids*, 2003, **15**(1), p 173-183
36. A.T.T. Tran and M.M. Hyland, The Role of Substrate Surface Chemistry on Splat Formation During Plasma Spray Deposition by Experiments and Simulations, Expanding Thermal Spray Performances to New Markets and Applications (*Proceedings of International Thermal Spray Conference 2009*), B.R. Marple, M.M. Hyland, Y.-C. Lau, C.-J. Li, R.S. Lima, and G. Montavon, Ed., 4-7 May 2009 (Las Vegas, NV), ASM International, 2009, p 462-468
37. S. Goutier, M. Vardelle, J.C. Labbe, and P. Fauchais, Alumina Splat Investigation: Visualization of Impact and Splat/Substrate Interface for Millimetre Sized Drops, Expanding Thermal Spray Performances to New Markets and Applications (*Proceedings of International Thermal Spray Conference 2009*), B.R. Marple, M.M. Hyland, Y.-C. Lau, C.-J. Li, R.S. Lima, and G. Montavon, Ed., 4-7 May 2009 (Las Vegas, NV), ASM International, 2009, p 883-888
38. M. Xue, S. Chandra, and J. Mostaghimi, Investigation of Splat Curling Up in Thermal Spray Coatings, *J. Therm. Spray Technol.*, 2006, **15**(4), p 531-536
39. A.T.T. Tran, M.M. Hyland, T. Qiu, B. Withy, and B.J. James, Effect of Surface Chemistry on Splat Formation During Plasma Spraying, Crossing Borders (*Proceedings of International Thermal Spray Conference 2008*), E. Lugscheider, Ed., 2-4 June 2008 (Maastricht, The Netherlands), ASM International, DVS-Verlag GmbH, 2008, p 701-706
40. J. Cedelle, M. Vardelle, and P. Fauchais, Influence of Stainless Steel Substrate Preheating on Surface Topography and on Millimeter- and Micrometer-Sized Splat Formation, *Surf. Coat. Technol.*, 2006, **201**, p 1373-1382